Spectral and Energy Efficiency Analysis of mmWave Communications with Channel Inversion in Outband D2D Network

Romain Chevillon, Guillaume Andrieux, Romain Négrier, Jean-François Diouris

Date of publication xxxx 00, 0000, date of current version xxxx 00, 0000.

Digital Object Identifier 10.1109/ACCESS.2017.DOI

Spectral and Energy Efficiency Analysis of mmWave Communications with Channel Inversion in Outband D2D Network

ROMAIN CHEVILLON, GUILLAUME ANDRIEUX, ROMAIN NÉGRIER, AND JEAN-FRANÇOIS DIOURIS.

Université Bretagne Loire, Université de Nantes, IUT de La Roche-sur-Yon, UMR 6164: Institute of Electronics and Telecommunications of Rennes (IETR), 18, boulevard Gaston-Defferre, 85035 La Roche-sur-Yon cedex, France

Corresponding author: Romain Chevillon (e-mail: romain.chevillon@univ-nantes.fr).

ABSTRACT Device-to-Device (D2D) communications is a promising approach for wireless communications in terms of energy and spectrum efficiency. However, such communications increase interferences in a cellular network. In this paper, we propose to lower these interferences by using millimeter wave directional antennas. To analyze the impact of these techniques, we introduce mathematical sectored antenna models that are deduced from mmWave antenna radiation patterns. Moreover, recent studies consider a constant transmit power for the devices. Nevertheless, modern communications use power control techniques to mitigate energy consumption and interferences. The main contribution of our work is the consideration of channel inversion, which is more realistic than the commonly used transmit model.

Most works dealing with conventional D2D communications propose to use stochastic geometry to model a D2D-enabled network in order to evaluate the impact of interferences and noise on the various links. The objective of this work is to analyze the SINR and the energy efficiency of Outband D2D links for UEs equipped with directional mmWave antennas. To do so, we implement an energy efficiency calculation that considers both directional antennas and channel inversion. We propose to highlight the advantages and drawbacks of directional mmWave antennas in Outband D2D for diverse antenna designs and different environments.

INDEX TERMS Device-to-device communication, Wireless communications, Stochastic processes, Radiofrequency interference, Multiple access interference, Millimeter wave communication, Directional antennas, Linear antenna arrays, Energy efficiency.

I. INTRODUCTION

DEVICE-TO-DEVICE (D2D) communications are viewed as a promising new technology and a keystone of the fifth generation of wireless networks (5G). D2D communications are based on the proximity between users, and permit to lower the battery usage for short distance transmissions [1]. D2D can be used for direct communications between devices and information relaying either between devices [2] or from a device to a base station (BS) [3]. For D2D communications, the synchronization between devices can be controlled either by the base station, or by the devices themselves [4].

A. RELATED WORKS

D2D spectrum sharing. In terms of spectrum sharing, D2D communications are mainly proposed to use the whole cellular spectrum (i.e. *Underlay Inband D2D*) [5]–[7]. Many approaches are proposed to decrease the impact of interference in Underlay Inband D2D, such as power control [8] or energy-efficient resource allocation [9]. Nevertheless, in order to avoid the interference between typical and D2D communications, some works propose to dedicate a part of the cellular spectrum for only D2D communications (i.e. *Overlay Inband D2D*) [10], [11]. Another approach based on non-cellular bands for D2D communications (i.e. *Outband D2D*) is also considered [12]. We focus on the later approach

in this paper to increase both the spectral efficiency and the energy efficiency of a whole network.

MmWave systems. Although biological safety [13] and channel behavior [14], [15] of mmWaves are not totally defined at the moment [16], the mmWave spectrum is a very interesting option for the next generation of wireless communications. Indeed, mmWave spectrum can support hundreds of times more capacity than the current cellular spectrum [1], [17]. In [18], the authors propose a system architecture based on mmWave and LTE. Their method introduces an effective resource sharing scheme that allows D2D links without interference. The authors of [12] propose to study the propagation in the mmWave spectrum (especially for bands in 24 GHz and 61 GHz) using ray tracing models in urban environments. Their results prove that mmWave approaches for D2D are highly achievable through beamforming. Indeed, these two methods decrease multipath interference due to urban structures. Besides, the authors of [1] and [19] reveal that the common buildings are very resistant to the penetration of mmWaves. In [20], the authors propose three user association strategies for mmWave D2D communications, and show that a "closest line-of-sight D2D-Tx" model is more spectrally efficient than the other ones (the comparison between each strategy is made thanks to stochastic geometry).

Blockage modeling. In mmWaves, the links from a D2D transmitter and a D2D receiver can be in a line-of-sight (LOS) state, in a non-line-of-sight (NLOS) state or in outage state [21]. If the link is in LOS state, the D2D transmitter is visible by the receiver, i.e. there is no blockage in the link [22]. However, if the link is in NLOS state, blockages occur between the transmitter and the receiver. If these blockages are too strong (i.e. if the path loss is very high), the link is considered as in outage state.

To model the blockage phenomenon, several approaches are depicted. First, a stochastic model is suggested by the 3GPP standards, differentiating LOS and NLOS links. These standards propose a function $P_{LOS}(d)$ that can be seen as the probability that a link of distance d is in LOS state. These functions differ for each environment (urban, rural, etc). They are explained in [23, Eqs. (1) and (2)]. Other authors like in [24] propose to model blockage with the help of random shape theory, taking into account that the centers of objects form a Poisson Point Process (PPP). The shape, size and orientation of each object are assumed to have a certain distribution. In addition to these two blockage modeling approaches, the LOS ball model has been introduced in [22], [25], [26]. In this model, the LOS probability function is modeled as a simple step function $P_{LOS} = \mathbb{1}(d < R_B)$, where R_B denotes the maximum length of a LOS link. In [27], the authors propose to model the blockage as a Boolean rectangle scheme. In [22], the authors adopt a D-ball approximation model. In our work, we propose to use the later approach. The model is explained in Section II. The authors of [28] leverage two-hop D2D relay to overcome blockages. All the calculations of coverage probabilities are made thanks to stochastic geometry.

Stochastic geometry. In terms of modeling, most works on D2D-enabled (D2D-e) networks use stochastic geometry to analyze power consumption, spectrum sharing and other characteristics [29]. In particular, the use of Point Processes such as PPP is significant in the works dealing with this topic. In [30], the authors introduce an empirical and analytical model of a D2D-e network, and demonstrate the SINR calculations related to their marked-PPP model. In [10], the authors adapt the results from [30] with the 3GPP propagation model. In [31], the authors use stochastic geometry to validate new spectrum access policies that may reduce interferences.

B. CONTRIBUTIONS AND ORGANIZATION

The related works dealing with stochastic geometry for D2D links mainly focus on Inband D2D communications, and consider only constant transmit powers. In this paper, we propose to analyze the advantages and the drawbacks of the use of mmWaves for Outband D2D communications with channel inversion. The main contributions of this paper are as follows:

- A D2D-e network model that considers channel inversion is introduced. This model is more realistic than the use of a constant transmit power. Modern communications use power control techniques to mitigate energy consumption and interferences. Channel inversion permits to adapt the transmission power relative to the link distance, the path-loss exponent and the Signal to Noise Ration (SNR). In this configuration, the SINR is optimized.
- Sectored antenna models are considered for Uniform Linear Array antennas (ULAs). They are probabilistically incorporated in the system model, from the antenna radiation patterns.
- An energy efficiency calculation that considers directional antennas is introduced. The energy efficiency is defined as the ratio of the spectral efficiency in an area to the average network power consumption.
- In our work, spectral and energy efficiencies for different types of ULAs (for 1, 3 and 5 elements) using their relative radiation pattern are compared.

Section II presents the system model. In Section III, we introduce the theoretical approach on mmWave directional antennas, based on linear array antennas theory. The analytical calculations for SINR (and more precisely the coverage probability) and energy efficiency are depicted in Section IV. The simulations and discussions are explained in Section V. Finally, conclusions are given in Section VI.

Notation: throughout the paper, $\mathbb{P}(\cdot)$ denotes the probability, $\mathbb{E}[\cdot]$ denotes the expectation over all random variables in $\{\cdot\}$, $\sim$ denotes the distribution and $\Gamma(a, b)$ denotes the Gamma distribution with parameters a and b, with a mean value of $a \cdot b$. The notation $\mathcal{L}_X(\cdot)$ defines the Laplace transform for the random variable X. The Euclidean norm is denoted as $\|\cdot\|$.

TABLE 1: Notation and Simulation Parameters

Parameter	Description	Value (if applicable)
	Network Model	
Φ_u	Set of the transmitter UEs with intensity λ_u	$\lambda_u = 2 \times \left(\pi 100^2\right)^{-1}$ m^{-2} (sparse) $\lambda_u = 20 \times \left(\pi 100^2\right)^{-1}$ m^{-2} (dense)
Φ_D	Set of the D2D UEs with intensity λ_D	$\lambda_D = q\lambda_u$
q	Potential D2D UEs	$q = 1$
X_i	Location of the *i*-th UE	
δ_i	Type of communication of the *i*-th UE	$\mathbb{P}(\delta_i = 1) = q$
L_i	Length of the D2D link of the *i*-th UE	$L_i = 25$ m
P_i	Transmitting power of the *i*-th UE	
θ_i	Oriented angle between the *i*-th transmitter and the *i*-th receiver	
	Small-scale Fading	
h_i	Small-scale fading on the *i*-th link	$h_i \sim \Gamma\left(N_L, \frac{1}{N_L}\right)$ (LOS-state link) $h_i \sim \Gamma\left(N_N, \frac{1}{N_N}\right)$ (NLOS-state link)
N_{L}	Parameter of Nakagami fading for LOS links	$N_{\mathrm{L}} = 3$
N_{N}	Parameter of Nakagami fading for NLOS links	$N_{\mathrm{N}} = 2$
	Blockage Model	
R_2, R_1	Radii of the approximating balls	$R_2 = 201.4371$ m $R_1 = 56.9945$ m
β_1	Probability that a link of length $r \in [0, D_1)$ is in LOS state	$\beta_1 = 0.8282$
β_2	Probability that a link of length $r \in [D_1, D_2)$ is in LOS state	$\beta_2 = 0.1216$
α_L	LOS pathloss exponents for mmWaves links	$\alpha_L = 2$
α_N	NLOS pathloss exponents for mmWaves links	$\alpha_N = 4$
$q_{d,L}$, $q_{d,N}$	Probability that a link in the d-th ball is in LOS or NLOS state	
$\mathcal{B}_d$	d-th ball with radius R_d	
	Antennas Models	
G	Antenna directivity gain	$G \in \{MM, Mm, mm\}$
p_G	Probability of the G antenna directivity gain	
$G_{i,j}$	Directivity gain between the *i*-th receiver and the *j*-th transmitter	$\mathbb{E}[G_{i,j}] = \sum_{G \in \{MM,Mm,mm\}} p_G G$
M, m	Antenna main lobe and side lobe gain	cf Table 3
Ω	Antenna main lobe beamwidth	cf Table 3
N_A	Number of ULA elementary antennas	$N_A \in \{1, 3, 5\}$
k_A	Wave vector	$k_A = 2\pi/\lambda_c$
d_A	Distance between each elementary isotropic antenna	$d_A = \lambda_c/2$
	Coverage Probability Metrics	
Ψ	SINR threshold	
Υ_i	SINR at a typical device	
	Energy Efficiency Metrics and Parameters	
P_0	Static power consumption of a UE	$P_0 = 343.8$ mW
$1/\Delta$	Efficiency of the UE power amplifier	$\Delta = 2$
P_{avg}	Average power consumption of UE per unit area	
τ	Area spectral efficiency	
EE	Energy efficiency	
	General Parameters	
W	Bandwidth	$W = 1$ GHz
F_c, λ_c	Carrier frequency and wavelength	$F_c = 28$ GHz, $\lambda_c = 10.7$ mm
σ^2	Noise power spectral density	$\sigma^2 = -174$ dBm/Hz

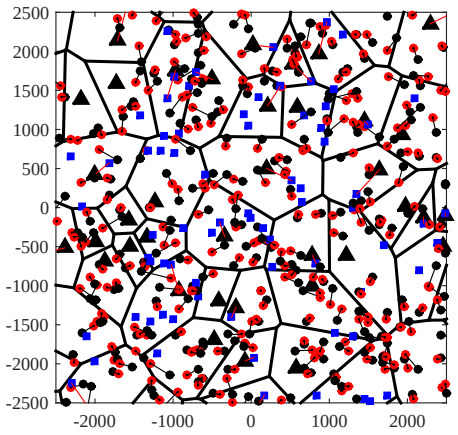

FIGURE 1: System model

II. SYSTEM MODEL

In this section, we introduce the system model through several assumptions. All the used notations and their relative description are given in Table 1.

Assumption 1 (PPP UE)

The user equipments (UE) are modeled by an independently marked PPP denoted as

$$\tilde{\Phi}_u = \{(X_i, \delta_i, L_i, P_i, \theta_i)\}, \tag{1}$$

where $\{X_i\}$, $\{\delta_i\}$, $\{L_i\}$, $\{P_i\}$ and $\{\theta_i\}$ denote the sets of the locations of the UEs, the type of communications for the UEs, the length of the D2D radio links (i.e. the distance between the transmitter and the receiver), the transmit power of the UEs and the angle between the D2D transmitter and receiver relative to the x-axis, respectively. $\{X_i\}$ are placed according to an unmarked PPP $\Phi_u \in \mathbb{R}^2$ with intensity λ_u. $\{\delta_i\}$ are assumed to be independent and identically distributed (i.i.d.) Bernoulli random variables with $\mathbb{P}(\delta_i = 1) = q$ [30], [32]. If $\delta_i = 1$, the UE i is considered as a potential D2D UE (so called DUE), otherwise, it is a cellular UE (so called CUE). In the following of this paper, we denote Φ_D the PPP of the DUEs, with intensity $\lambda_D = q\lambda_u$. Moreover, $\{\theta_i\}$ are assumed to be uniformly distributed within $(0, 2\pi]$. The position of the UEs are shown in Fig. 1.

Assumption 2 (D2D Distance)

In this paper, we assume that the distance between two elements of a D2D pair is constant for all the pairs, as modeled in recent works like [33]–[35]. Then, for all the pairs, we take $L_i = 25$ m, that is a decent value for D2D links [33], [36]. Note that we also assume that all the D2D links are active.

Assumption 3 (Small-Scale Fading)

As explained in [19], [23], the Rayleigh fading model used in sub-6 GHz band cannot be applied for mmWave communications. Indeed, in [27], the authors recommend to assume independent Nakagami fading for each link. The parameters of Nakagami fading for LOS and NLOS are denoted as N_L and N_N, respectively (assuming N_L and N_N are positive integers). If h_i is the small-scale fading term on the i-th link, h_i is a normalized Gamma random variable ($h_i \sim \Gamma\left(N_L, \frac{1}{N_L}\right)$ or $h_i \sim \Gamma\left(N_N, \frac{1}{N_N}\right)$). Frequency selectivity in fading is not considered in this paper. Indeed, measurements made in [19] clearly show that the delay spread is relatively small, and the frequency-selective fading can have a limited impact using techniques like OFDM or frequency domain equalization [37]. Moreover, the measurement results in [19] show that small-scale fading at mmWaves is less severe than that in LTE systems when narrow beam antennas are used.

Assumption 4 (Blockage Process and Path Loss Model)

The blockages, e.g. buildings in cities, form a process of random shapes on the plane [27]. The distribution of the blockage process (modeled by a stochastic model [23]) is assumed to be stationary and isotropic. We adopt the generalized LOS D-ball model approximation explained in [22] and validated in [23] as the most realistic blockage model among all others, like those explained in [37] or [38]. The D-ball model approximation is shown in Fig. 2. In this model, a link is in LOS state with probability $q_{1,L} = \beta_1$ inside the first ball with radius R_1, while this link is in NLOS state with probability $q_{1,N} = 1 - \beta_1$. Similarly, the LOS probability for a link is equal to $q_{d,L} = \beta_d$ if the distance between a transmitter and a receiver is comprised between R_{d-1} and R_d for $d = 2, \ldots, D$. All the links with distances greater than R_D are assumed to be in outage state [22].

Moreover, the path loss laws are different for LOS and NLOS links. The path loss on each link can be expressed as in (2), where α_L and α_N are the LOS and the NLOS path loss exponents for all the balls [22].

In the following of this paper, $\mathcal{B}_1$ corresponds to the first ball with radius R_1, and $\mathcal{B}_d$ corresponds to the area comprised between the $(d-1)$-th ball (with radius R_{d-1}) and the d-th ball (with radius R_d).

Assumption 5 (Directional Beamforming Modeling)

We assume analog beamforming is applied at both D2D transmitters and receivers. The D2D transmitter and its associated receiver have a perfect channel knowledge, and then adjust their steering orientation so as to achieve the maximum directionality gain [23]. In the following of this paper, we denote $G_{i,j}$ the effective antenna gain between the i-th receiver and the j-th transmitter. Therefore, for a desired D2D signal link, perfect beam pointing is assumed with $G_{i,i} = G_0$.

The steering angles of the interfering DUEs are assumed to be uniformly distributed within $(0, 2\pi]$. For simplicity, the actual patterns are approximated by sectored models. Note that the sectored models for directive antennas are depicted in Section III.

$$\nu(r) = \begin{cases} \begin{cases} r^{\alpha_L} & \text{w/ prob. } q_{1,L} = \beta_1 \\ r^{\alpha_N} & \text{w/ prob. } q_{1,N} = (1-\beta_1) \end{cases} & \text{if } r \in [0, R_1) \\ \begin{cases} r^{\alpha_L} & \text{w/ prob. } q_{2,L} = \beta_2 \\ r^{\alpha_N} & \text{w/ prob. } q_{2,N} = (1-\beta_2) \end{cases} & \text{if } r \in [R_1, R_2) \\ \vdots & \\ \begin{cases} r^{\alpha_L} & \text{w/ prob. } q_{D,L} = \beta_{\mathrm{D}} \\ r^{\alpha_N} & \text{w/ prob. } q_{D,N} = (1-\beta_{\mathrm{D}}) \end{cases} & \text{if } r \in \left[R_{(D-1)}, R_D\right) \\ \text{outage} & \text{if } r \geq R_D. \end{cases} \tag{2}$$

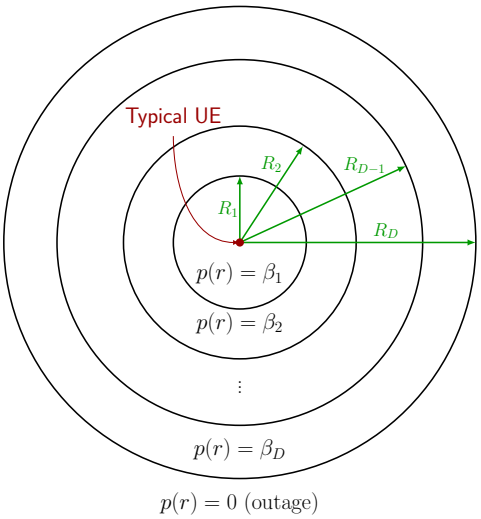

FIGURE 2: D-ball approximation model

Assumption 6 (Channel Inversion-Based Power Control and Normalized Antenna Gain)

The received power at a typical D2D receiver from its transmitter is $P_{u,i} = P_i G_0 L_i^{-\alpha_s} h_i$, with $s \in \{L, N\}$. We assume channel inversion based power control and normalized antenna gain, i.e. $P_{u,i} = h_i$ and thus $P_i = L_i^{\alpha_s}$ and $G_0 = 1$.

III. MM-WAVES AND DIRECTIONAL ANTENNAS MODELING

We consider the Outband D2D communications use the mmWave spectrum, with the help of directional antennas. Similarly to the works [39] and [12], the operating frequency is $F_c = 28\,\mathrm{GHz}$, then the wavelength is $\lambda_c = 10.7\,\mathrm{mm}$.

A. MMWAVE ANTENNA ARRAY

Let us consider a Uniform Linear Array (ULA) composed of N_A isotropic antennas [40] at both the transmitter and the receiver.

All the elementary isotropic antennas composing the array are separated by a distance d_A. The mmWave antenna array is described in Fig. 3. In this figure, θ_A denotes the angle of departure of the mmWave to the receiver.

Note that we assume that the receiver is in the far field of the transmitter, and the elements of the linear array antennas are mechanically aligned in order to perform electronically synthetic pattern.

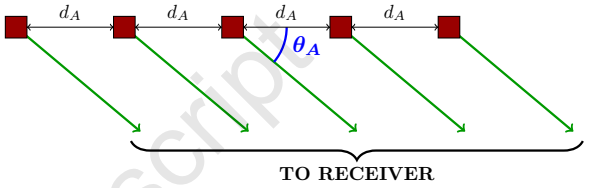

FIGURE 3: ULA. The red squares and green lines denote the elementary antennas and the rays, respectively.

The array factor $\mathrm{AF}\left(\theta_A, N_A, d_A\right)$ for an N_A-antenna array with identically excited elements is defined by

$$\mathrm{AF}\left(\theta_A, N_A, d_A\right) = \sum_{n=1}^{N_A} e^{j(n-1)(k_A d_A \cos\theta_A)} \tag{3}$$

where $k_A = 2\pi/\lambda_c$ denotes the wave vector [41, Chap. 6.3].

The reference point is the physical center of the ULA. Then, the radiation pattern $\zeta\left(\theta_A, N_A, d_A\right)$ of the array factor can be expressed as follows:

$$\zeta\left(\theta_A, N_A, d_A\right) = \left| \frac{\sin\left(N_A k_A d_A \cos\left(\theta_A\right)/2\right)}{\sin\left(k_A d_A \cos\left(\theta_A\right)/2\right)} \right| \tag{4}$$

In terms of power, $\zeta^2\left(\theta_A, N_A, d_A\right)$ represents the directivity of the array. This is due to the fact that elementary antennas are omnidirectional. The normalized radiation pattern (in terms of power) is shown in Fig. 4 (a), (b) and (c).

In this work, we took a value of $d_A = \lambda_c/2 = 5.35\,\mathrm{mm}$.

Remarks on directivity, radiated power and transmitting power

For a non-normalized radiation pattern, the maximum directivity is expressed as in (5) [41] with $\zeta^*\left(\theta_A, N_A, \varphi, d_A\right)$ given in (6). For $d_A = \lambda_c/2$, (5) can be simplified by $D_{max}\left(N_A, d_A\right) = N_A$. The power of the typical link signal received by DUE i is $P_{u,i} = P_i L_i^{-\alpha} G_0 h_i$. Note that the receiver and the transmitter antenna gains are given by the directivity of the antennas. Moreover, as explained before, we consider that the antennas are mechanically aligned. Thus, both receiver and transmitter antennas provide a gain equal

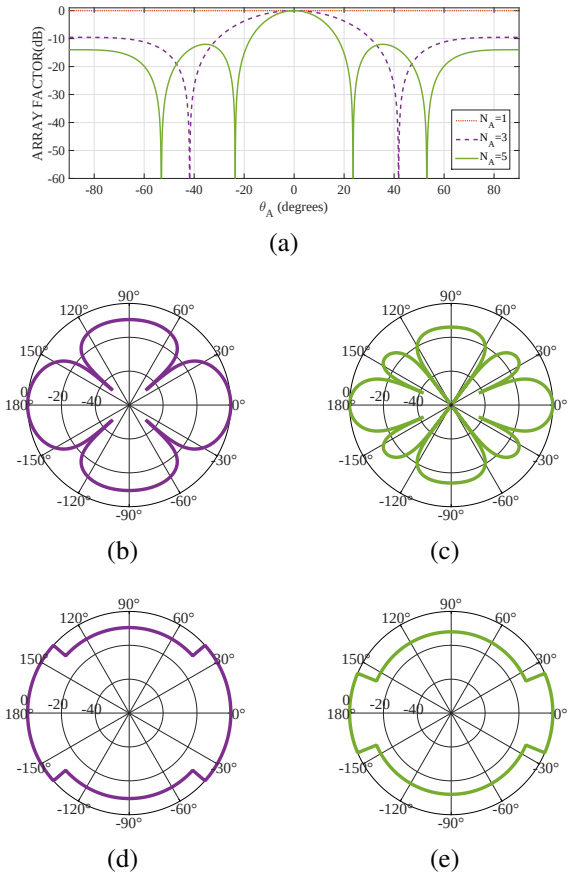

FIGURE 4: Normalized radiation pattern of N_A-antenna array. (a) Array Factor in dB for N_A=1, 3 and 5. (b) Polar plot of relative directivity with N_A=3. (c) Polar plot of relative directivity with N_A=5. (d) Sectored-pattern antenna model for N_A=3. (e) Sectored-pattern antenna model for N_A=5.

to the maximum directivity (i.e. $G_0 = D_{max}(N_A, d_A)$). With $d_A = \lambda_c/2$, we thus have $P_{u,i} = P_i L_i^{-\alpha} N_A^2 h_i$.

Recall that we use power channel inversion. Then, $P_i = \frac{L_i^{\alpha}}{N_A^2}$. This equality clearly shows that the transmission power can be highly reduced if we add elementary antennas to the ULA. Numerically, by replacing an isotropic antenna by a 4 element array, the total transmitting power can be diminished by 12dB. Thus, we can say that the use of directional antennas allows to highly increase the energy efficiency of D2D links, and, subsequently, of the whole array.

B. TRANSMITTER AND RECEIVER BEAMFORMING

Enhancement of the link budget is established by aligning both the transmitter and receiver main lobes. First, each UE periodically transmits and receives discovery signals ("beacons") [42]. The beacons are sent with the help of omnidirectional antennas. When the beacon relative to a D2D communication is received, the use of ULA permits to estimate the angle of arrival of the wave coming from the D2D transmitter. Then, the transmitter and the receiver align their main lobes with a beamforming method. This approach

TABLE 2: Probability Mass Function of G [23], [27]

G	MM	Mm	mm
p_G	$(c_{UE})^2$	$2c_{UE}(1-c_{UE})$	$(1-c_{UE})^2$

TABLE 3: Effective antenna gain between an interfering D2D transmitter and a D2D receiver

ULA type	M	m	Ω
ULA-1	0 dBi	N.A.	N.A.
ULA-3	0 dBi	-9.54 dBi	2.93 rad
ULA-5	0 dBi	-12.04 dBi	1.61 rad

is described in [14].

C. SECTORED-PATTERN ULA ANTENNA MODEL

In this paper, we propose to use sectored-pattern antenna models, as in [22], [23], [27]. In this model, the actual array beam pattern is approximated by a step function with a constant main lobe over the beam width and a constant side lobe otherwise. The accuracy of this model has been validated by [43] and [44]. Thus, the main lobe gain of the ULA antenna is assumed to be equal to M for all the angles in the -3 dB main lobe, and to m otherwise. Because of beamforming (as explained in Section II, Assumption 5), the overall antenna gain of a D2D pair is $G_0 = MM$. Moreover, the beam direction of the interfering links is modeled as a uniform random variable distributed within $(0, 2\pi]$. Then the effective antenna gain between an interfering D2D transmitter and a D2D receiver is a discrete random variable as described in Table 2 [22], where G is the effective directivity gain, Ω is the -3 dB beam width of the main lobe, and p_G is the probability of having an effective antenna gain of $G \in \{MM, Mm, mm\}$ (where $c_{UE} = \frac{\Omega}{2\pi}$). The sectored-pattern antenna models for ULA-3 and ULA-5 are shown in Fig. 4 (d) and (e). The numerical values of M, m and Ω for ULA-1, ULA-3 and ULA-5 are given in Table 3.

In the following of this paper, we denote $G_{i,j}$ the directivity gain between the i-th receiver and the j-th transmitter. For an interfering link, the average directivity gain can be written as follows:

$$\mathbb{E}[G_{i,j}] = \sum_{G \in \{MM, Mm, mm\}} p_G G. \quad (7)$$

Note that $G_{i,j}$ corresponds to a typical link directivity gain, while G denotes the effective directivity gain.

IV. COVERAGE AND ENERGY EFFICIENCY ANALYSIS

In this section, we consider mmWave based channels. We consider a D2D pair DP_i comprising a transmitter $\mathrm{D}_{t,i}$ and a receiver $\mathrm{D}_{r,i}$. The baseband received signal by $\mathrm{D}_{r,i}$ can be written as follows:

$$D_{max}\left(N_A, d_A\right) = 4\pi \frac{N_A^2}{\int_0^{\pi}\int_0^{2\pi} \zeta^*\left(\theta_A, N_A, \varphi, d_A\right) d\varphi d\theta} \tag{5}$$

$$\zeta^*\left(\theta_A, N_A, \varphi, d_A\right) = \left(\frac{\sin\left(N_A k_A d_A \sin\left(\theta_A\right)\cos\left(\varphi\right)/2\right)}{\sin\left(k_A d_A \sin\left(\theta_A\right)\cos\left(\varphi\right)/2\right)}\right)^2 \sin\left(\theta\right) \tag{6}$$

$$\begin{aligned} Y_i[n] =& \sqrt{P_i L_i^{-\alpha_s} G_0 h_i} S_i[n] \\ &+ \sum_{X_j \in \Phi_{D,I^{(i)}}} \sqrt{P_j L_{i,j}^{-\alpha_s} G_{i,j} h_{i\leftarrow j}} S_j[n] \\ &+ Z[n], \end{aligned} \tag{8}$$

with $s \in \{L, N\}$ and where h_i, S_i, $\Phi_{D,I^{(i)}}$, $L_{i,j}$, $h_{i\leftarrow j}$, S_j and $Z[n]$ denote the small-scale fading of the typical link, the unit-variance signal of the typical link, the set of the devices that interfere with the i-th device, the distance between the j-th transmitter and the i-th receiver, the small-scale fading between the j-th transmitter and the i-th receiver, the unit-variance signal of the j-th interfering link and the Additive White Gaussian Noise (AWGN), respectively.

A. INTERFERENCES CHARACTERIZATION

The objective of this section is to characterize all the interferences undergone by a typical D2D receiver in a LOS D-ball model.

First, we consider a D2D link where the co-channel interferences are generated by the potential D2D UEs operating in D2D mode [45]. We assume the typical DUE receiver is located at the origin of the space. Furthermore, we assume that the typical link length L_i is comprised in the d-th ball $\mathcal{B}_d$. Therefore, the typical link is either in LOS state, with a probability β_d, or in NLOS-state, with a probability $1-\beta_d$.

The first interferers on the typical link are those placed in the first ball $\mathcal{B}_1$ (i.e. those that located at a distance to the typical receiver comprised between 0 and R_1). The link between the typical DUE and the interferers can be in LOS state, or in NLOS-state, with probabilities β_1 or $1-\beta_1$, respectively. Moreover, recall that the link between an interferer's receiver and its related transmitter can be in LOS or in NLOS. As we use channel inversion, $P_{u,j} = h_j$, then $P_j = L_j^{\alpha_s}$, with $s \in \{L, N\}$. Thus, the set of the interferers in the first ball comprises (i) the set of the interferers with a LOS state link to the typical link and a LOS state link between their own receiver and transmitter $\Phi_{D,L,L} \cap \mathcal{B}_1$, (ii) the set of the interferers with a LOS state link to the typical link and a NLOS state link between their own receiver and transmitter $\Phi_{D,L,N} \cap \mathcal{B}_1$, (iii) the set of the interferers with a NLOS state link to the typical link and a LOS state link between their own receiver and transmitter $\Phi_{D,N,L} \cap \mathcal{B}_1$ and (iv) the set of the interferers with a NLOS state link to the typical link and a NLOS state link between their own receiver and transmitter $\Phi_{D,N,N} \cap \mathcal{B}_1$.

Similarly, the set of the interferers in the d-th ball comprises the same four cases depicted for the first ball (i.e. $\Phi_{D,L,L} \cap \mathcal{B}_d$, $\Phi_{D,L,N} \cap \mathcal{B}_d$, $\Phi_{D,N,L} \cap \mathcal{B}_d$ and $\Phi_{D,N,N} \cap \mathcal{B}_d$). Then, the sum of the interferences $I_{agg,d}$ in the d-th ball can be expressed as in (9).

The aggregated interferences undergone by the typical device corresponds to the sum of all the interferences for all the balls. Subsequently, the aggregated interferences at a typical DUE is given by (10).

B. SINR CHARACTERIZATION

The signal-to-interference-plus-noise ratio (SINR) at a typical DUE can be written as

$$\Upsilon_i = \frac{P_{u,i}}{I_{agg} + P_n}, \tag{11}$$

where $P_n = \sigma^2 \cdot W$, $\sigma^2 = -174\,\mathrm{dBm/Hz}$ and W denote the power of the noise at the typical device, the noise power spectral density and the bandwidth, respectively. As a result, by taking into account Assumption 6,

$$\Upsilon_{\mathrm{i}} = \frac{h_i}{\sum_{d=1}^{D} I_{agg,d} + P_n}. \tag{12}$$

Note on channel inversion

In this paper, we consider channel inversion. This implies that the transmit power is calculated with respect to the distance between the transmitter and the receiver (nevertheless, it does not take into account the fading). In other words, $P_{u,i} = h_i$. The SNR (Signal to Noise Ratio) defined as the average received signal power normalized by noise power [30] is expressed as (for the i-th device):

$$\mathrm{SNR}_i = \frac{P_i L_i^{-\alpha_s}}{P_n}, \tag{13}$$

with $s \in \{L, N\}$, and thus $P_n = \frac{1}{\mathrm{SNR}}$. Note that we consider the power of noise is similar for each device.

C. COVERAGE PROBABILITY

The Complementary Cumulative Distribution Function (CCDF) of the SINR representing the probability that the SINR is larger or equal to Ψ, as known as Coverage Probability, can be written :

$$
\begin{aligned}
I_{agg,d} = & \sum_{X_j \in \Phi_{D,L,L} \cap \mathcal{B}_d} h_j G_{i,j} L_j^{\alpha_L} \left\| X_j \right\|^{-\alpha_L} + \sum_{X_j \in \Phi_{D,L,N} \cap \mathcal{B}_d} h_j G_{i,j} L_j^{\alpha_N} \left\| X_j \right\|^{-\alpha_L} \\
& + \sum_{X_j \in \Phi_{D,N,L} \cap \mathcal{B}_d} h_j G_{i,j} L_j^{\alpha_L} \left\| X_j \right\|^{-\alpha_N} + \sum_{X_j \in \Phi_{D,N,N} \cap \mathcal{B}_d} h_j G_{i,j} L_j^{\alpha_N} \left\| X_j \right\|^{-\alpha_N} \\
= & \sum_{s_1 \in \{L,N\}} \sum_{s_2 \in \{L,N\}} \sum_{X_j \in \Phi_{D,s_1,s_2} \cap \mathcal{B}_d} h_j G_{i,j} L_j^{\alpha_{s_2}} \left\| X_j \right\|^{-\alpha_{s_1}} . \qquad (9)
\end{aligned}
$$

$$
I_{agg} = \sum_{d=1}^{D} I_{agg,d} = \sum_{d=1}^{D} \sum_{s_1 \in \{L,N\}} \sum_{s_2 \in \{L,N\}} \sum_{X_j \in \Phi_{D,s_1,s_2} \cap \mathcal{B}_d} h_j G_{i,j} L_j^{\alpha_{s_2}} \left\| X_j \right\|^{-\alpha_{s_1}} . \qquad (10)
$$

$$
\begin{aligned}
\mathcal{C}(\Psi) &= \mathbb{P}\left(\frac{h_i}{I_{agg} + P_n} \geq \Psi \right) \\
&= \mathbb{P}\left(h_i \geq \Psi \left(I_{agg} + P_n \right) \right) . \qquad (14)
\end{aligned}
$$

1) Conditional Coverage Probabilities

We clearly see in (14) that the coverage probability depends on the small-scale fading parameter h_i that is different for LOS and NLOS links. Thus, the overall coverage probability can be written as follows:

$$
\mathcal{C}(\Psi) = \mathbb{P}_L \mathcal{C}_L(\Psi) + \mathbb{P}_N \mathcal{C}_N(\Psi) \qquad (15)
$$

where $\mathbb{P}_L$, $\mathbb{P}_N$, $\mathcal{C}_L(\Psi)$ and $\mathcal{C}_N(\Psi)$ denote the probability that the typical link is in LOS (i.e. $h_i \sim \Gamma\left(N_L, \frac{1}{N_L}\right)$), the probability that the typical link is in NLOS (i.e. $h_i \sim \Gamma\left(N_N, \frac{1}{N_N}\right)$), the conditional coverage probability if the link is in LOS and the conditional coverage probability if the link is in NLOS.

The analytical values of $\mathbb{P}_L$ and $\mathbb{P}_N$ can be found using (2), and is written as in (16).

Lemma 1. *For a s state link (with $s \in \{L, N\}$), the conditional coverage probability is given as follows:*

$$
\mathcal{C}_s(\Psi) = \sum_{n=1}^{N_s} (-1)^{n+1} \binom{N_s}{n} e^{-u_s P_n} \mathcal{L}_{I_{agg}}(u_s), \qquad (17)
$$

where $u_s = n\eta_s \Psi$, $\eta_s = N_s \left(N_s!\right)^{-\frac{1}{N_s}}$ and $\mathcal{L}_{I_{agg}}(u_s)$ denotes the Laplace transform of the aggregated interferences for a s state link.

Proof: See Appendix A. ■

Lemma 2. *The Laplace transform of the aggregated interferences can be written as in (18), where $\mathbb{E}\left[P^{(s)}\right]$ denotes the average transmit power of a DUE, with $s \in \{L, N\}$.*

Proof: See Appendix B. ■

Theorem 3. *From Lemmas 1 and 2, we can say that the overall Coverage Probability is written as in (19).*

D. ENERGY EFFICIENCY

1) Power Consumption

The power consumption of each UE implies two components: the static power P_0 and the transmit power P_t.

According to [46], the static power comprises the CPU consumption, the battery consumption, among others, and the display consumption. The average static power consumption is 343.8 mW.

Moreover, as we have seen before, we use channel inversion with a 10 dB SNR. Thus, the power of the typical signal $P_{u,i}$ received by the DUE receiver is 10 times higher than the power of the noise P_n, where $P_n = W \times \sigma^2$: $P_{u,i} = \text{SNR} \times W \times \sigma^2$. Subsequently, the power emitted by the transmitter in the direction of its receiver is $P_{e,0} = P_{u,i} L_i^{\alpha_s}$, with $s \in \{L, N\}$. Then, the average power emitted by a transmitter in the exact direction of its receiver is given as follows:

$$
P_{e,avg} = P_{u,i} \sum_{d=1}^{D} \sum_{s \in \{L,N\}} q_{d,s} L_i^{-\alpha_s} \qquad (20)
$$

Therefore, the transmit power of the device is given by (21).

Subsequently, the total power consumption P_{tot} of a UE can be written $P_{tot} = P_0 + \Delta P_t$, where $1/\Delta$ is the efficiency of the power amplifier [22], [47]. Then, the average power consumption per unit area of UEs can be given by (22).

2) Energy Efficiency

We define the area spectral efficiency τ as the product of the throughput of a given link and the density of UEs [22]. Then,

$$
\tau = \lambda_D \mathcal{C}\left(\Psi\right) \log_2\left(1 + \Psi\right) . \qquad (23)
$$

This metric allows to calculate the energy efficiency, which is defined as the ratio of the area spectral efficiency to the average network power consumption, and is given by (24).

V. SIMULATIONS AND DISCUSSIONS

The parameters used in the following simulations are given in Table 1. We consider that the D2D communications are using mmWaves at 28 GHz. Moreover, we assume a 2-ball model

$$\begin{cases} \mathbb{P}_L &= \mathbb{P}\left[L_i \in [0, R_1)\right] \beta_1 + \sum_{d=2}^{D} \mathbb{P}\left[L_i \in [R_{d-1}, R_d)\right] \beta_d, \\ \mathbb{P}_N &= \mathbb{P}\left[L_i \in [0, R_1)\right] (1-\beta_1) + \sum_{d=2}^{D} \mathbb{P}\left[L_i \in [R_{d-1}, R_d)\right] (1-\beta_d). \end{cases} \tag{16}$$

$$\mathcal{L}_{I_{agg}}(u) = \prod_{G\in\{MM,Mm,mm\}} \prod_{d=1}^{D} \prod_{s_1\in\{L,N\}} \prod_{s_2\in\{L,N\}} \exp\left(-2\pi\lambda_D \cdot p_G \cdot q_{d,s_1} \cdot q_{d,s_2} \int_{\mathcal{B}_d} \left(1 - \left(1 + u\mathbb{E}\left[P^{(s_2)}\right] \frac{r^{-\alpha_{s_1}}}{N_{s_1}}\right)^{-N_{s_1}}\right) r\mathrm{d}r\right). \tag{18}$$

$$\mathcal{C}(\Psi) = \sum_{s\in\{L,N\}} \left(\mathbb{P}_s \prod_{G\in\{MM,Mm,mm\}} \prod_{d=1}^{D} \prod_{s_1\in\{L,N\}} \prod_{s_2\in\{L,N\}} \exp\left(-2\pi\lambda_D \cdot p_G \cdot q_{d,s_1} \cdot q_{d,s_2} \int_{\mathcal{B}_d} \left(1 - \left(1 + u_s\mathbb{E}\left[P^{(s_2)}\right] \frac{r^{-\alpha_{s_1}}}{N_{s_1}}\right)^{-N_{s_1}}\right) r\mathrm{d}r\right)\right). \tag{19}$$

$$P_t = \frac{P_{u,i}}{N_A} \int_0^{2\pi} \zeta^2\left(\theta_A, N_A, d_A\right) \mathrm{d}\theta_A \times \left(\sum_{d=1}^{D} \sum_{s\in\{L,N\}} q_{d,s} L_i^{-\alpha_s}\right). \tag{21}$$

for blockage, as depicted in [22], [37]. The simulations are made with a 10.000 round Monte-Carlo method.

We propose to analyze the coverage probability and the energy efficiency for SNR=10 dB. We consider that the maximum coverage distance is the same for both values of SNR. We also consider that the linear array antennas have 1, 3 and 5 elements. Indeed, for a 5 element linear array, the total antenna width is around 75 mm, which is appropriate for a typical UE.

A. SPARSE NETWORK

1) Coverage Probability

Fig. 5 shows the CCDF of SINR for D2D links for mmWaves in a network with $\lambda_D = 2 \times \left(\pi 100^2\right)^{-1}$ m^{-2}.

First of all, we can see that the analytical results are highly validated with the Monte-Carlo simulations. Nevertheless, the difference between the simulations and the theoretical results comes from the approximation in the calculation of the Laplace transform of the aggregated interferences given in Lemma 2.

We clearly see that the coverage probability converges to the value of 1 if $\Psi \to -\infty$ for all the antenna models. Nevertheless, this convergence is slower for low numbers of elements. Indeed, for $N_A = 1$, the coverage probability of 1 is reached for $\Psi = -35$ dB, whereas for $N_A = 5$, this value is reached for $\Psi = -23$ dB. This result is mainly due to the directivity of the ULA. Indeed, the main lobe is narrower for ULA-5 than for ULA-1. Thus, the aggregated number of interferences that come from main lobe antennas is decreased, as well as the power of interferences. This improvement of SINR due to directive ULA antennas can be seen for each SINR threshold: Fig. 5 shows a maximum difference of 0.16 for the coverage probability between ULA-1 and ULA-5.

However, the difference between ULA-3 and ULA-5 is quite thin (maximum difference of 0.08) for every SINR threshold. This result is due to the fact that in a sparse network, i.e. with a low λ_D, the impact of p_G, for $G \in \{MM, Mm, mm\}$, is not very high. This difference can be calculated and easily proven with the numerical values given in Table 3.

Finally, we can see the presence of a "step" in the coverage probability. This step is clear for ULA-1, for $\Psi \in (-4\,\mathrm{dB}, -9\,\mathrm{dB})$, and is mainly due to the 2-LOS ball blockage modeling. Actually, the blockage is more important for omnidirectional antennas, as the power is emitted with the same intensity in all directions. Thus, there is no attenuation, and the LOS-ball model is more preponderant than with directive antennas, for which the side lobes attenuate the signal. Moreover, the low density of devices permit to have this step (as the attenuation is more tangible than in a high density of devices). This can be seen by comparing with Fig. 7.

2) Energy Efficiency

Fig. 6 shows the energy efficiency (EE) for D2D links in a sparse network. This EE is obtained from (24). We clearly see that the maximum EE values for each case are different. The best EE is obtained for ULA-5 (which is not really surprising), and reaches a value of $0.83\,\mathrm{bps/Hz/W}$ for $\Psi = 6.1$. It

$$P_{avg} = \lambda_D \left(P_0 + \Delta \frac{P_{u,i}}{N_A} \int_0^{2\pi} \zeta^2 \left(\theta_A, N_A, d_A\right) \mathrm{d}\theta_A \times \left(\sum_{d=1}^{D} \sum_{s \in \{L,N\}} q_{d,s} L_i^{-\alpha_s} \right) \right). \tag{22}$$

$$\mathrm{EE} = \frac{\tau}{P_{avg}} = \frac{\mathcal{C}\left(\Psi\right) \log_2\left(1+\Psi\right)}{P_0 + \Delta \frac{1}{N_A} \int_0^{2\pi} \zeta^2 \left(\theta_A, N_A, d_A\right) \mathrm{d}\theta_A \times \left(\sum_{d=1}^{D} \sum_{s \in \{L,N\}} q_{d,s} L_i^{-\alpha_s} \right)}. \tag{24}$$

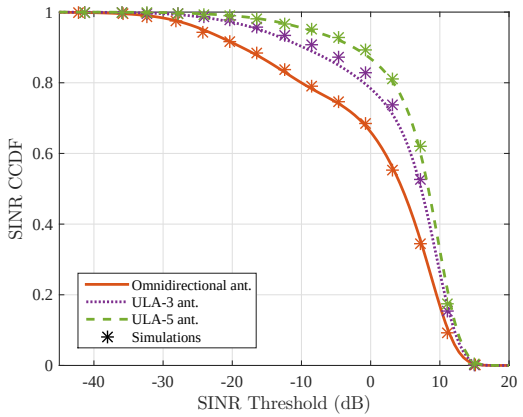

FIGURE 5: Analytical and simulation values of CCDF of SINR for D2D links with mmWave ULA in a sparse network, with $\lambda_D = 2 \times \left(\pi 100^2\right)^{-1}$ m^{-2} for $N_A = 1$, $N_A = 3$ and $N_A = 5$.

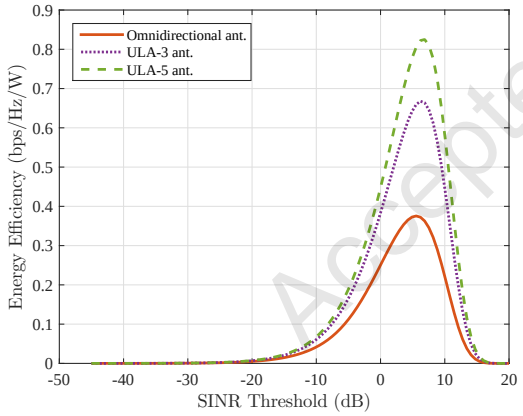

FIGURE 6: Energy Efficiency for D2D links with mmWave ULA in a sparse network, with $\lambda_D = 2 \times \left(\pi 100^2\right)^{-1}$ m^{-2}, for $N_A = 1$, $N_A = 3$ and $N_A = 5$.

is 0.16bps/Hz/W better than the maximum value for ULA-3 and 0.45 bps/Hz/W better than the maximum value for ULA-1 (more than 2.3 times higher).

We also see in this figure that the maximum energy efficiency is not reached for the same threshold for all cases. It can be proven mathematically by calculating numerically $\frac{\partial \mathrm{EE}}{\partial \Psi}$, and more precisely $\frac{\partial \mathcal{C}(\Psi)}{\partial \Psi}$. Indeed, for ULA-1, the maximum value is reached for $\Psi = 4.8$ dB. For ULA-3, it is reached for $\Psi = 5.2$ dB, and for ULA-5, it is reached for $\Psi = 6.1$ dB.

Figs. 5 and 6 show that the use of directive ULA antennas in sparse network is interesting, both in terms of SINR and energy efficiency. Nevertheless, in this case, the use of high number of elements antennas (i.e. more than 4) is not necessary. Indeed, the cost of the ULA would be increased, but the benefits in terms of spectral and energy efficiencies are not so interesting. Thus, for sparse network applications, we would recommend a ULA-3 to have a good compromise between spectral efficiency, energy efficiency and antenna cost.

B. DENSE NETWORK

1) Coverage Probability

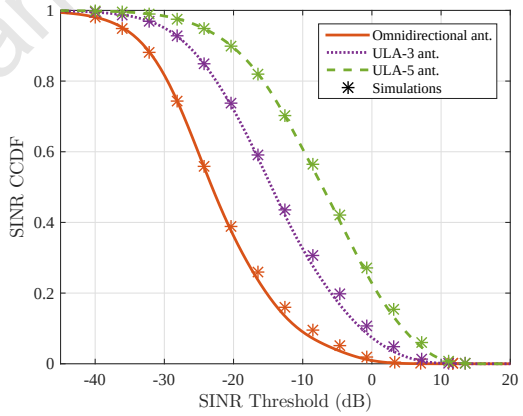

FIGURE 7: CCDF of SINR for D2D links with mmWave ULA in a dense network, with $\lambda_D = 20 \times \left(\pi 100^2\right)^{-1}$ m^{-2}, for $N_A = 1$, $N_A = 3$ and $N_A = 5$.

Fig. 7 shows the coverage probability for D2D links in a dense network. We clearly see that the simulations and theoretical results fit better than for a sparse network, which is due to the high number of devices. As the density is greater than in the first case, the approximation in the calculation of $\mathcal{L}_{I_{agg}}$ for a Nakagami-m small-scale fading model is less preponderant.

We clearly see that the difference in the coverage probability increases between each case compared to a sparse network. Indeed, the higher difference in coverage probability between ULA-3 and ULA-5 is 0.2, while between ULA-1 and ULA-5, this value reaches 0.45. Moreover, for a SINR threshold of -10 dB in a sparse network, the difference in terms of coverage probability between the omnidirectional antenna model and the ULA-3 model is 0.11, whereas in a

dense network, this difference equals 0.23. Similarly, in a sparse network, the difference in terms of coverage probability between the omnidirectional antenna model and the ULA-5 model is 0.15, whereas in a dense network, this difference equals 0.52. This is mainly due to the following two important aspects.

1) The number of devices is bigger, then the number of aggregated interferences is higher, and then the attenuation due to the ULA is more tangible.
2) The density is higher, then the distance between a typical device and its interferers is decreased compared to a sparse network. Thus, the number of interfering devices located in the 2-LOS ball is bigger, as well as the impact of the antennas attenuation.

The maximum difference of SINR between ULA-1 and ULA-5 is 16 dB, which is very high. This difference will undoubtedly lead to a huge difference in EE, as shown in Fig. 8.

2) Energy Efficiency

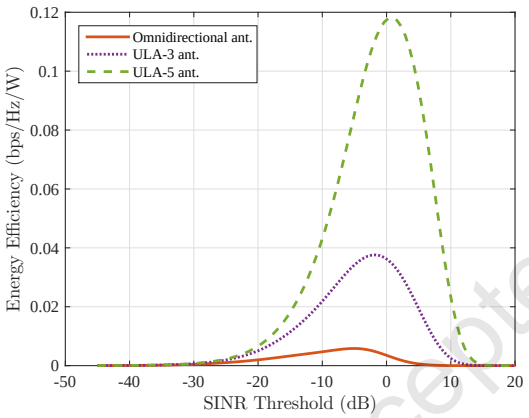

FIGURE 8: Energy Efficiency for D2D links with mmWave ULA in a dense network, with $\lambda_D = 20 \times \left(\pi 100^2\right)^{-1}$ m^{-2}, for $N_A = 1$, $N_A = 3$ and $N_A = 5$.

The energy efficiency for D2D links in a dense network is shown in Fig. 8. As for a sparse network, the best EE is obtained for ULA-5, and reaches a value of $0.118\mathrm{bps/Hz/W}$ for $\Psi = 0.1$ dB. It is 0.08 bps/Hz/W better than the maximum value for ULA-3 and 0.11 bps/Hz/W better than the maximum value for ULA-1 (more than 23 times higher).

As in sparse network, the maximum energy efficiency is not reached for the same Ψ for all cases. For ULA-1, the maximum value is reached for $\Psi = -4.9$ dB, for ULA-3, it is reached for $\Psi = -1.7$ dB, and for ULA-5, it is reached for $\Psi = 0.1$ dB.

Figs. 7 and 8 clearly show that the use of directive ULA antennas in dense network is of great importance, and even necessary. First, in terms of coverage probability, the use of ULA-5 is very interesting. It permits to increase the SINR by 16 dB compared to ULA-1. But the main interest in the use of ULA resides in the energy efficiency. Indeed, the use of an uniform linear antenna with 5 elements permits to have an energy efficiency that is more than 23 times better than with an omnidirectional antenna. This means that the throughput is increased, and the battery consumption is decreased.

Increasing the number of ULA elements can provide better results, but at the price of practical and physical limitations.

VI. CONCLUSION

In this paper we have introduced mmWave directional antennas in Outband D2D links. We have analyzed the possible advantages of such a technology in a D2D-enabled network. The analysis has been based on stochastic geometry theory and linear array antenna design. We have proved that despite the fact that mmWaves imply smaller coverage areas than with conventional communications, the use of this technology can considerably improve the spectral efficiency (SINR) of an Outband D2D network. Subsequently, the energy efficiency can be highly improved by using multiple element directional antennas. Indeed, the energy efficiency can be increased by a factor 23 in a dense network with a ULA-5, compared to an omnidirectional antenna. High number of elements in mmWave ULAs is really interesting for D2D communications (in terms of spectral efficiency and energy efficiency), in particular for dense urban environments. However, the use of more than 3 element ULAs is not really necessary for sparse networks in terms of energy efficiency.

.

APPENDIX A PROOF OF LEMMA 1

The conditional coverage probability of a threshold Ψ can be calculated as follows:

$$\mathcal{C}_s(\Psi) = \mathbb{P}\left(\frac{h_i}{I_{agg}+P_n} \geq \Psi\right) \tag{25}$$

$$= \mathbb{P}\left(h_i \geq \Psi\left(I_{agg}+P_n\right)\right) \tag{26}$$

$$\overset{(a)}{\approx} 1 - \mathbb{E}_{\Phi_{D,s}}\left[\left(1-e^{-\eta_s \Psi\left(I_{agg}+P_n\right)}\right)\right] \tag{27}$$

$$\overset{(b)}{=} \sum_{n=1}^{N_s} (-1)^{n+1} \binom{N_s}{n} \mathbb{E}_{\Phi_{D,s}}\left[e^{-n\eta_s \Psi\left(I_{agg}+P_n\right)}\right] \tag{28}$$

$$\overset{(c)}{=} \sum_{n=1}^{N_s} (-1)^{n+1} \binom{N_s}{n} e^{-n\eta_s \Psi P_n} \mathcal{L}_{I_{agg}}\left(n\eta_s \Psi\right), \tag{29}$$

where $N_s \in \{N_L, N_N\}$, $\eta_s = N_s \left(N_s!\right)^{-\frac{1}{N_s}}$ (with $s \in \{L, N\}$), (a) is from [48], (b) comes from the fact that N_s is an integer and from the Binomial theorem, and (c) follows from the fact that the noise power and the power of the aggregated interferences are independent random values.

APPENDIX B PROOF OF LEMMA 2

The Laplace transform of the aggregated interferences can be calculated as in (30), where (a) comes from the definition of the Laplace transform of I_{agg}, (b) follows from

$$\mathcal{L}_{I_{agg}}(u) = \mathbb{E}\left[e^{-uI_{agg}}\right] \tag{30}$$

$$\overset{(a)}{=} \mathbb{E}_{h,G,\Phi_{D,s_1},\Phi_{D,s_2}}\left[\exp\left(-u\left(\sum_{d=1}^{D}\sum_{s_1\in\{L,N\}}\sum_{s_2\in\{L,N\}}\sum_{X_j\in\Phi_{D,s_1,s_2}\cap\mathcal{B}_d} h_j G_{i,j} L_j^{\alpha_{s_2}} \left\|X_j\right\|^{-\alpha_{s_1}}\right)\right)\right]$$

$$\overset{(b)}{=} \mathbb{E}_{G,\Phi_{D,s_2}}\left[\exp\left(-2\pi\lambda_D\left(\sum_{d=1}^{D}\sum_{s_1\in\{L,N\}}\sum_{s_2\in\{L,N\}}\sum_{X_j\in\Phi_{D,s_1,s_2}\cap\mathcal{B}_d} q_{d,s_1}\left(1-\left(1+\frac{uG_{i,j}L_j^{\alpha_{s_2}}\left\|X_j\right\|^{-\alpha_{s_1}}}{N_{s_1}}\right)^{-N_{s_1}}\right)\right)\right)\right]$$

$$\overset{(c)}{=} \mathbb{E}_{\Phi_{D,s_2}}\left[\exp\left(-2\pi\lambda_D\left(\sum_{G\in\{MM,Mm,mm\}} p_G \sum_{d=1}^{D}\sum_{s_1\in\{L,N\}}\sum_{s_2\in\{L,N\}}\sum_{X_j\in\Phi_{D,s_1,s_2}\cap\mathcal{B}_d} q_{d,s_1}\left(1-\left(1+\frac{uGL_j^{\alpha_{s_2}}\left\|X_j\right\|^{-\alpha_{s_1}}}{N_{s_1}}\right)^{-N_{s_1}}\right)\right)\right)\right]$$

$$\overset{(d)}{=} \exp\left(-2\pi\lambda_D\left(\sum_{G\in\{MM,Mm,mm\}} p_G \sum_{d=1}^{D}\sum_{s_1\in\{L,N\}}\sum_{s_2\in\{L,N\}} q_{d,s_1}q_{d,s_2}\int_{\mathcal{B}_d}\left(1-\left(1+\frac{uG\mathbb{E}\left[P^{(s_2)}\right]r^{-\alpha_{s_1}}}{N_{s_1}}\right)^{-N_{s_1}}\right)r\mathrm{d}r\right)\right), \tag{31}$$

the moment-generating function of a Gamma distribution (as $h_j \sim \Gamma\left(N_s, \frac{1}{N_s}\right)$), (c) follows from the independence between all the variables, and (d) follows from the fact that each D2D link has the same length. This leads to the result in Lemma 2.

ACKNOWLEDGMENT

This work was supported by RFS company through University of Nantes Foundation, Région Pays-de-la-Loire, Conseil Départemental de la Vendée and La Roche-sur-Yon Agglomération.

REFERENCES

[1] M. Agiwal, A. Roy, and N. Saxena, "Next Generation 5G Wireless Networks: A Comprehensive Survey," IEEE Communications Surveys & Tutorials, vol. 18, no. 3, pp. 1617 – 1655, 2016.

[2] R. Chevillon, G. Andrieux, and J.-F. Diouris, "Energy Optimization of D2D Communications Using Relay Devices and Data Entropy," in 2017 IEEE 28th Annual International Symposium on Personal, Indoor, and Mobile Radio Communications (PIMRC), Montréal, Canada, 2017.

[3] A. Gupta and R. K. Jha, "A Survey of 5G Network: Architecture and Emerging Technologies," IEEE Access, vol. 3, pp. 1206–1232, 2015.

[4] M. N. Tehrani, M. Uysal, and H. Yanikomeroglu, "Device-to-device communication in 5G cellular networks: challenges, solutions, and future directions," IEEE Communications Magazine, vol. 52, no. 5, pp. 86–92, 2014.

[5] A. Asadi, Q. Wang, and V. Mancuso, "A survey on device-to-device communication in cellular networks," IEEE Communications Surveys and Tutorials, vol. 16, no. 4, pp. 1801–1819, 2014.

[6] Z. Zhou, M. Dong, K. Ota, J. Wu, and T. Sato, "Energy Efficiency and Spectral Efficiency Tradeoff in Device-to-Device (D2D) Communications," IEEE Wireless Communications Letters, vol. 3, no. 5, pp. 485–488, Oct 2014.

[7] A. Bhardwaj and S. Agnihotri, "Energy- and Spectral-Efficiency Trade-Off for D2D-Multicasts in Underlay Cellular Networks," IEEE Wireless Communications Letters, vol. 7, no. 4, pp. 546–549, Aug 2018.

[8] A. He, L. Wang, Y. Chen, K. Wong, and M. Elkashlan, "Spectral and Energy Efficiency of Uplink D2D Underlaid Massive MIMO Cellular Networks," IEEE Transactions on Communications, vol. 65, no. 9, pp. 3780–3793, Sept 2017.

[9] Z. Zhou, M. Dong, K. Ota, G. Wang, and L. T. Yang, "Energy-Efficient Resource Allocation for D2D Communications Underlaying Cloud-RAN-Based LTE-A Networks," IEEE Internet of Things Journal, vol. 3, no. 3, pp. 428–438, June 2016.

[10] A. Afzal, S. Ali, R. Zaidi, D. McLernon, and M. Ghogho, "On the Analysis of Device-to-Device Overlaid Cellular Networks in the Uplink under 3GPP Propagation Model," in IEEE Wireless Communications and Networking Conference, 2016, pp. 1–6.

[11] J. Liu, N. Kato, J. Ma, and N. Kadowaki, "Device-to-Device Communication in LTE-Advanced Networks: A Survey," IEEE Communications Surveys and Tutorials, vol. 17, no. 4, pp. 1923–1940, 2015.

[12] A. Al-Hourani, S. Chandrasekharan, and S. Kandeepan, "Path loss study for millimeter wave device-to-device communications in urban environment," 2014 IEEE International Conference on Communications Workshops, ICC 2014, pp. 102–107, 2014.

[13] T. Wu and T. S. Rappaport, "Safe for generations to come: considerations of safety for millimeter waves in wireless communications," IEEE Microwave Magazine, vol. 16, no. 2, pp. 65–84, 2015.

[14] W. Roh, J. Y. Seol, J. Park, B. Lee, J. Lee, Y. Kim, J. Cho, K. Cheun, and F. Aryanfar, "Millimeter-wave beamforming as an enabling technology for 5G cellular communications: theoretical feasibility and prototype results," IEEE Communications Magazine, vol. 52, no. 2, pp. 106–113, 2014.

[15] M. Kyro, V. Kolmonen and P. Vainikainen, "Experimental propagation channel characterization of mm-wave radio links in urban scenarios," IEEE Antennas Wireless Propagation Letters, vol. 11, no. July, pp. 865–868, 2012.

[16] M. Ji, G. Caire, and A. Molisch, "Wireless device-to-device caching networks: Basic principles and system performance," IEEE Journal on Selected Areas in Communications, vol. 34, no. 1, pp. 176–189, 2016.

[17] J. G. Andrews, S. Buzzi, W. Choi, S. V. Hanly, A. Lozano, A. C. K. Soong,

and J. C. Zhang, "What Will 5G Be ?" IEEE Journal on Selected Areas in Communications, vol. 32, no. 6, pp. 1065–1082, 2014.
[18] J. Qiao, X. Shen, J. W. Mark, Q. Shen, Y. He, and L. Lei, "Enabling Device-to-Device Communications in Millimeter-Wave 5G Cellular Networks," IEEE Communications Magazine, no. January, pp. 209–215, 2015.
[19] T. S. Rappaport, S. H. U. Sun, R. Mayzus, H. Zhao, Y. Azar, K. Wang, G. N. Wong, J. K. Schulz, M. Samimi, and F. Gutierrez, "Millimeter Wave Mobile Communications for 5G Cellular : It Will Work !" IEEE Access, vol. 1, pp. 335–349, 2013.
[20] W. Yi, Y. Liu, and A. Nallanathan, "Modeling and Analysis of D2D Millimeter-Wave," vol. 65, no. 12, pp. 5574–5588, 2017.
[21] M. R. Akdeniz, Y. Liu, M. K. Samimi, S. Sun, S. Rangan, T. S. Rappaport, and E. Erkip, "Millimeter wave channel modeling and cellular capacity evaluation," IEEE Journal on Selected Areas in Communications, vol. 32, no. 6, pp. 1164–1179, 2014.
[22] E. Turgut and M. C. Gursoy, "Coverage in Heterogeneous Downlink Millimeter Wave Cellular Networks," IEEE Transactions on Communications, vol. 65, no. 10, pp. 4463–4477, 2017.
[23] J. G. Andrews, T. Bai, M. Kulkarni, A. Alkhateeb, A. Gupta, and R. W. Heath, "Modeling and Analyzing Millimeter Wave Cellular Systems," IEEE Transactions on Communications, vol. 65, no. 1, pp. 403–430, 2017.
[24] T. Bai, R. Vaze, and R. W. Heath, "Analysis of blockage effects on urban cellular networks," IEEE Transactions on Wireless Communications, vol. 13, no. 9, pp. 5070–5083, 2014.
[25] W. Lu and M. D. Renzo, "Stochastic Geometry Modeling of Cellular Networks: Analysis, Simulation and Experimental Validation," pp. 1–4, 2015. [Online]. Available: http://arxiv.org/abs/1506.0385
[26] S. Singh, M. N. Kulkarni, A. Ghosh, and J. G. Andrews, "Tractable Model for Rate in Self-Backhauled Millimeter Wave Cellular Networks," IEEE Journal on Selected Areas in Communications, vol. 33, no. 10, pp. 2191–2211, 2015.
[27] T. Bai and R. W. Heath, "Coverage and Rate Analysis for Millimeter Wave Cellular Networks," IEEE Transactions on Wireless Communications, vol. 14, no. 2, pp. 1100–1114, 2015.
[28] S. Wu, S. Member, R. Atat, and S. Member, "Improving the Coverage and Spectral Efficiency of Millimeter-Wave Cellular Networks Using Device-to-Device Relays," vol. 66, no. 5, pp. 2251–2265, 2018.
[29] M. Haenggi, J. G. Andrews, F. Baccelli, O. Dousse, and M. Franceschetti, "Stochastic Geometry and Random Graphs for the Analysis and Design of Wireless Networks," IEEE Journal on Selected Areas in Communications, vol. 27, no. 7, pp. 1029–1046, 2009.
[30] X. Lin, J. G. Andrews, and A. Ghosh, "Spectrum sharing for device-to-device communication in cellular networks," IEEE Transactions on Wireless Communications, vol. 13, no. 12, pp. 6727–6740, 2014.
[31] A. H. Sakr, E. Hossain, and N. I. May, "Cognitive and Energy Harvesting-Based D2D Communication in Cellular Networks : Stochastic Geometry Modeling and Analysis," IEEE Transactions on Communications, vol. 63, no. 5, pp. 1–13, 2015.
[32] R. Chevillon, G. Andrieux, R. Négrier, and J.-F. Diouris, "Effects of Directional Antennas on Outband D2D mmWave Communications in Heterogeneous Networks," AEU - International Journal of Electronics and Communications, vol. 96, pp. 58 – 65, 2018.
[33] H. Ghavami and S. S. Moghaddam, "Outage Probability of Device to Device Communications Underlaying Cellular Network in Suzuki Fading Channel," IEEE Communications Letters, vol. 21, no. 5, pp. 1203–1206, 2017.
[34] Y. Zhang, Y. Xu, M. Gao, Q. Zhang, H. Li, I. Ahmad, and Z. Feng, "Resource Management in Device-to-Device Underlaying Cellular Network," 2015 IEEE Wireless Communications and Networking Conference (WCNC), pp. 1649–1654, 2015.
[35] H. Zhang, L. Song, and Z. Han, "Radio Resource Allocation for Device-to-Device Underlay Communication Using Hypergraph Theory," IEEE Transactions on Wireless Communications, vol. 15, no. 7, pp. 4852–4861, 2016.
[36] A. Thornburg, T. Bai, and R. W. Heath, "Performance Analysis of Outdoor mmWave Adhoc Networks," IEEE Transactions on Signal Processing, vol. 64, no. 15, pp. 4065–4079, 2016.
[37] M. Di Renzo, "Stochastic Geometry Modeling and Analysis of Multi-Tier Millimeter Wave Cellular Networks," IEEE Transactions on Wireless Communications, vol. 14, no. 9, pp. 5038–5057, 2015.
[38] H. ElSawy, A. Sultan-Salem, M.-S. Alouini, and M. Z. Win, "Modeling and Analysis of Cellular Networks Using Stochastic Geometry: A Tutorial," IEEE Communications Surveys & Tutorials, vol. 19, no. 1, pp. 167–203, 2017.
[39] G. R. Maccartney, J. Zhang, S. Nie, and T. S. Rappaport, "Path loss models for 5G millimeter wave propagation channels in urban microcells," GLOBECOM - IEEE Global Telecommunications Conference, pp. 3948–3953, 2013.
[40] M. Soszka, S. Berger, A. Fehske, M. Simsek, B. Butkiewicz, and G. Fettweis, "Coverage and Capacity Optimization in Cellular Radio Networks with Advanced Antennas," in WSA 2015; 19th International ITG Workshop on Smart Antennas, 2015, pp. 1–6.
[41] C. A. Balanis, Antenna Theory, Analysis and Design - Third Edition. Wiley New York, 2005.
[42] C. Choi, S. Park, and D. H. Cho, "User-cooperation scheme based on clustering for energy efficiency in cellular networks with D2D communication," in IEEE International Symposium on Personal, Indoor and Mobile Radio Communications, PIMRC, vol. 1, 2014, pp. 1365–1369.
[43] A. Alkhateeb, Y. H. Nam, M. S. Rahman, J. Zhang, and R. W. Heath, "Initial Beam Association in Millimeter Wave Cellular Systems: Analysis and Design Insights," IEEE Transactions on Wireless Communications, vol. 16, no. 5, pp. 2807–2821, 2017.
[44] T. Bai, A. Alkhateeb, and R. Heath, "Coverage and capacity of millimeter-wave cellular networks," IEEE Communications Magazine, vol. 52, no. 9, pp. 70–77, 2014.
[45] Y. J. Chun, S. L. Cotton, H. S. Dhillon, A. Ghrayeb, and M. O. Hasna, "A Stochastic Geometric Analysis of Device-to-Device Communications Operating Over Generalized Fading Channels," IEEE Transactions on Wireless Communications, vol. 16, no. 7, pp. 4151–4165, 2017.
[46] A. Carroll and G. Heiser, "An analysis of power consumption in a smartphone," Proceedings of the 2010 USENIX conference on USENIX annual technical conference, pp. 21–35, 2010.
[47] S. C. Cripps, RF Power Amplifiers for Wireless Communications, 2nd ed. Artech House, 2006.
[48] H. Alzer, "On Some Inequalities for the Incomplete Gamma Function," Mathematics of Computation, vol. 66, no. 218, p. 312, 1997.

ROMAIN CHEVILLON was born in La Roche-sur-Yon, France, in 1985. He received the Dipl.-Ing. degree in Electronics and Computer Science from the Ecole Polytechnique de l'Université de Nantes (France) in 2008. During his scholarship, he specialized in Acoustics and Advanced Applied Mathematics at the Technical University of Denmark in Kongens-Lyngby (Denmark). After spending three years in the music industry, he worked during four years as a Research Coordinator in the domains of Music Information Retrieval (MIR) and Cyber Security. He integrated the Institute of Electronics and Telecommunications of Rennes (IETR), University of Nantes, in 2015 as a PhD student. His research domains are mainly energy and spectral efficiencies in Device-to-Device communications and heterogeneous networks, and stochastic geometry.

GUILLAUME ANDRIEUX received the M.S. degree in Telecommunications and the Ph.D. degree in electrical engineering from the University of Nantes, France, in 2000 and 2004, respectively. He is currently an Associate Professor at the Networks and Telecommunications Department, University of Nantes. His current research interests are digital communications, antenna processing, energy efficiency in wireless networks and channel estimation.

ROMAIN NÉGRIER received the Ph.D. degree in telecommunications engineering from the University of Limoges, Limoges, France, in 2016. For nearly a year, he worked as a research engineer with IETR in the Antennas and Microwave Devices Department, University of Nantes, France. He is currently an Associate Professor with the XLIM research institute, University of Limoges, Limoges, France. His research interests include wireless sensor network, ultrawideband radar system and associated processing.

JEAN-FRANÇOIS DIOURIS received his PhD degrees from University of Rennes I, France, in 1991. He is currently professor at Polytech Nantes, University of Nantes, France and adjunct director of Institute of Electronics and Telecommunications of Rennes. His current research interests are digital communications, antenna processing and energy efficient communications.